Open access • Journal Article • DOI:10.1109/5.867692

Fully embedded board-level guided-wave optoelectronic interconnects

Ray T. Chen, Lei Lin, Chulchae Choi, Yujie Liu ...+8 more authors

Institutions: Cray, Honeywell, General Electric

Published on: 01 Jun 2000

Topics: Waveguide (optics), Clock signal, Optical communication, Printed circuit board and Integrated circuit

Fully Embedded Board-Level Guided-Wave Optoelectronic Interconnects

RAY T. CHEN, SENIOR MEMBER, IEEE, LEI LIN, CHULCHAE CHOI, YUJIE J. LIU, BIPIN BIHARI, L. WU, SUNING TANG, MEMBER, IEEE, R. WICKMAN, B. PICOR, M. K. HIBBS-BRENNER, J. BRISTOW, AND Y. S. LIU

Invited Paper

A fully embedded board-level guided-wave optical interconnection is presented to solve the packaging compatibility problem. All elements involved in providing high-speed optical communications within one board are demonstrated. Experimental results on a 12-channel linear array of thin-film polyimide waveguides, vertical-cavity surface-emitting lasers (VCSEL's) (42 μm), and silicon MSM photodetectors (10 μm) suitable for a fully embedded implementation are provided. Two types of waveguide couplers, titled gratings and 45° total internal reflection mirrors, are fabricated within the polyimide waveguides. Thirty-five to near 100% coupling efficiencies are experimentally confirmed. By doing so, all the real estate of the PC board surface are occupied by electronics, and therefore one only observes the performance enhancement due to the employment of optical interconnection but does not worry about the interface problem between electronic and optoelectronic components unlike conventional approaches.

A high speed 1–48 optical clock signal distribution network for Cray T-90 supercomputer is demonstrated. A waveguide propagation loss of 0.21 dB/cm at 850 nm was experimentally confirmed for the 1–48 clock signal distribution and for point-to-point interconnects. The feasibility of using polyimide as the interlayer dielectric material to form hybrid three-dimensional interconnects is also demonstrated. Finally, a waveguide bus architecture is presented, which provides a realistic bidirectional broadcasting transmission of optical signals. Such a structure is equivalent to such IEEE standard bus protocols as VME bus and FutureBus$^+$.

Manuscript received August 25, 1999; revised February 23, 2000. This work was supported by ONR, BMDO, DARPA, the State of Texas under the ATP Program, the 3M Foundation, Dell Computer, Cray Research, GE, Honeywell, and MCC.

R. T. Chen, L. Lin, C. Choi, Y. J. Liu, B. Bihari, and L. Wu are with the Microelectronics Research Center, University of Texas, Austin, TX 78758 USA.

S. Tang is with Radiant Research, Austin, TX 78758 USA.

R. Wickman and B. Picor are with Cray Research, Chippewa, WI 54729 USA.

M. K. Hibbs-Brenner, J. Bristow are with the Honeywell Technology Center, Minneapolis, MN 55418 USA.

Y. S. Liu is with the GE Research and Development Center, Schenectady, NY 12345 USA.

Publisher Item Identifier S 0018-9219(00)05931-4.

Keywords*—*Imbedded structures, micromirror couplers, MSM detectors, optical backplane bus, optoelectronic interconnects, polymeric waveguides, VCSEL, VMEbus.

I. INTRODUCTION

The speed and complexity of integrated circuits are increased rapidly as integrated circuit technology advances from very large-scale integrated (VLSI) circuits to ultra-large-scale integrated (ULSI) circuits. As the number of components per chip, the number of chips per board, the modulation speed, and the degree of integration continue to increase, electrical interconnects are facing their fundamental bottlenecks, such as speed, packaging, fanout, and power dissipation. Multichip module (MCM) technology is employed to provide higher data transfer rates and circuit densities [1], [2]. The employment of copper and lower dielectric constant materials can release the bottleneck for next several years. However, the interconnection roadmap published by Sematech still predicts a major bottleneck by 2006 [3]. The employment of optical interconnects will be one of the major alternatives for upgrading the interconnection speed whenever conventional electrical interconnection fails to provide the required bandwidth.

Machine-to-machine interconnection has already been significantly replaced by optical means. The major research thrusts in optical interconnection are in the backplane and board level where the interconnection distance, the associated parasitic RLC effects, and the large fanout induced impedance mismatch are to jeopardize the bandwidth requirements. Optical interconnection has been widely agreed as a better alternative to upgrade the system performance. However, reliability and packaging compatibility of many demonstrated optical interconnect systems [4]–[6] have impeded the integration of optical interconnect into a real

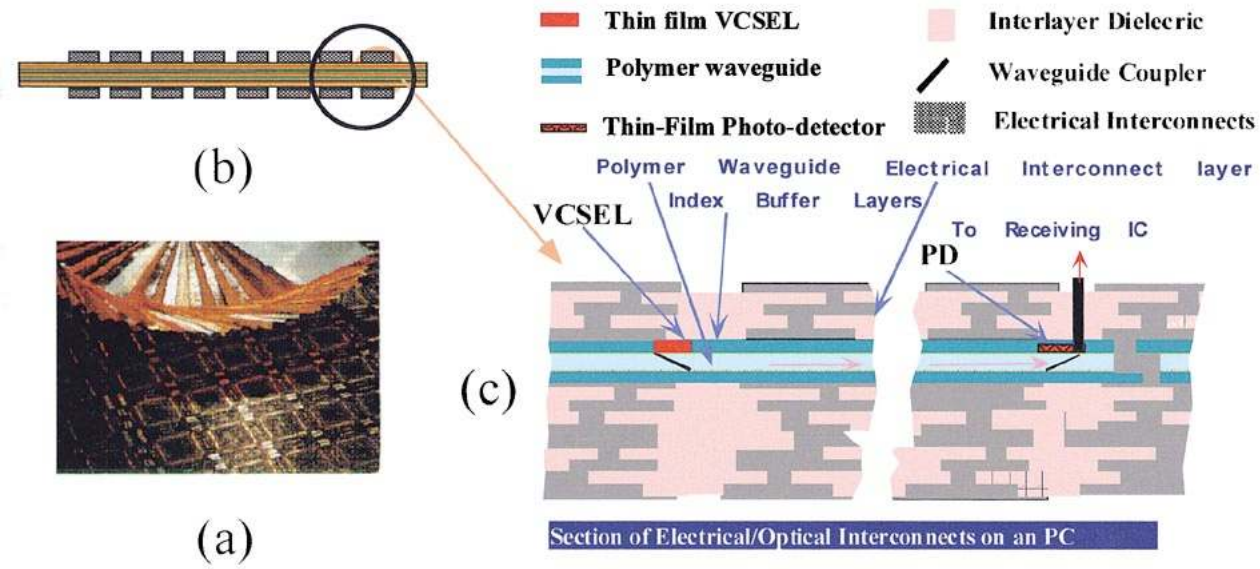

Fig. 1. The fully embedded guided wave optical interconnect system architecture. (a) 52 vertical integration layers of a supercomputer board, (b) schematic of the side view of the vertical integration layers, and (c) details of the schematic shown in (b). Waveguides, VCSEL, photodetector, waveguide coupler, electrical vias, and other electrical interconnection layers are clearly shown.

system. For example, the board-level optical interconnections reported in [4] are all using hybrid approach where both electronic and optoelectronic components are located at the surface of the board. Such an approach makes the packaging difficult and costly. Furthermore, the employment of free space instead of guided-wave optical interconnection reported in [4]–[6] makes the system vulnerable in harsh environment.

In this paper, we present a new system architecture to solve these problems and the experimental results aimed at fulfilling such an architecture. In contrast to previous approaches, a fully embedded board-level guided-wave optical interconnection is presented in Fig. 1, where all elements involved in providing high-speed optical communications within one board are shown. These include a vertical-cavity surface-emitting laser (VCSEL), surface-normal waveguide couplers, and a polyimide-based channel waveguide functioning as the physical layer of optical bus and a photoreceiver. The driving electrical signal to modulate the VCSEL and the demodulated signal received at the photoreceiver are all through electrical vias connecting to the surface of the PC board. By doing so, all the real estate of the PC board surface are occupied by electronics, and therefore one only observes the performance enhancement due to the employment of optical interconnection but does not worry about the interface problem between electronic and optoelectronic components, unlike conventional approaches.

To provide the needed building blocks for the architecture shown in Fig. 1, the research findings of polyimide-based waveguides, waveguide couplers, high-speed thin-film transmitters using VCSEL's, and thin-film receivers operating at 850 nm are presented sequentially in this paper. The fully embedded structure makes the insertion of optoelectronic components into microelectronic systems much more realistic when considering the fact that the major stumbling block for implementing optical interconnection onto high-performance microelectronics is the packaging incompatibility. The research work presented herein eventually will release such a concern and make the integration of optical interconnection highly feasible. A board level 1–48 clock signal distribution for Cray-T-90 supercomputer board is demonstrated with a speed of 6 Gbit/s. The formation of three-dimensional (3-D) interconnection using polyimide as the interlayer dielectric material is further demonstrated to ensure the feasibility of the proposed idea. Finally, a polymer-based optical bus structure is presented with full compatibility with existing board-level IEEE-standardized buses such as VME bus and FutureBus.

II. Polymer Waveguides

To provide system integration using guided-wave optical interconnection, polymer-based material has its exclusive advantages. It can be spin-coated on a myriad of substrates with a relatively large interconnection distance. A large variety of organic polymers are attractive as microelectronic and optoelectronic materials with potential applications as interlayer dielectric, protective overcoat, α-ray shielding, optical interconnects, or even conductive electrical interconnects. In addition to their ease of processing, they possess favorable electrical and mechanical properties such as high resistivity, low dielectric constant, light weight, and flexibility. Compatibility with the microelectronic fabrication, however, is the thermal requirement for the polymer material to survive wire-bonding and metal deposition processes. A specialized class of polyimides stands out in this aspect, as they exhibit thermal stability to above 400 °C.

The polyimide PMDA/ODA, prepared from pyromellitic dianhydride and 4,4′-oxidianiline, is a typical commercially available polyimide coating. Kapton, the first aromatic

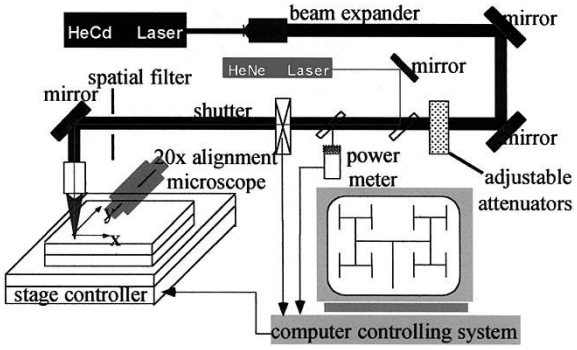

Fig. 2. Schematic setup for direct laser beam writing for polyimide waveguide formation.

polyimide commercialized by DuPont in 1960, is physically stable over a wide range of temperatures (−270 °C–400 °C), has excellent heat resistance and chemical resistance and therefore provides the required high-temperature process compatibility.

For optical interconnect applications, PMDA/ODA and other rigid rod polyimides are not the best candidates. They are anisotropic and also tend to be highly colored due to intramolecular charge transfer complexes that form between the electron rich diamine and electron deficient dianhydride. These properties result in high optical absorption and scattering losses. Recent investigations to produce "colorless" polyimides by interrupting the planarity of the polyimide chain have focused on polyimides based on 2,2-bis (dicarboxyphenyl) hexafluoropropane dianhydride (6FDA), into which the hexafluoro group has been incorporated to reduce the optical anisotropy.

For board-level interconnection, the interconnection distance can be easily in the range of tens of centimeters. For example, the Cray T-90 supercomputer board is 26.67 cm in length [7], which is beyond the field size of the in-house microlithography. Large-area optical waveguides are required to build an optical clock signal distribution layer. To meet the size requirement, a laser beam direct writing was employed to solve the problem. The laser-beam writing system consists of a dual-wavelength HeCd laser ($\lambda_1 = 325$ nm and $\lambda_2 = 442$ nm), beam-shaping optics, an electronic shuttle, and a computer-controlled X-Y-Z translation stage with a stroke of $30 \times 30 \times 2.5$ cm^3. The stage translation speed was continuously adjustable below 1.0 cm/s. The positioning resolution is 0.5 and 0.01 μm for the X-Y axes and Z-axis, respectively. The Z-stage was employed to precisely control the focused laser beam sizes. Fig. 2 shows the schematic diagram of the laser writing system for channel waveguide formation.

To ensure the desired electrical and mechanical properties imposed on board-level optical interconnection, and to meet the required optical properties for the low-loss waveguide formation, the photosensitive polyimide provided by Amoco Chemicals was used for the waveguide fabrication [24]. The polyimides employed have excellent thermal stability ($Tg = 400$ °C) and optical transparency when they are thermally or photochemically cross-linked. To fabricate the channel waveguides, the photosensitive polyimide was first spin-coated on the substrate, followed by a soft-cure process to remove the solvent. The exposure was conducted by a focused HeCd UV laser beam ($\lambda = 325$ nm) writing, directed by a computer-controlled X-Y-Z precision microtranslation stage. The photo-crosslinked polyimide film was finally etched using organic solvent developers into the desired channel patterns. The fabricated waveguides was postbaked at 300 °C–350 °C to remove residual solvent and to improve the solvent resistance.

Fig. 3(a) is the photograph of a 1-to-2 3-dB waveguide splitter based on polyimide channel waveguides fabricated with a channel width of 50 μm, which is compatible with the core size of a multimode glass fiber. The waveguide thickness is measured to be 10 μm. Fig. 3(b) is a curved waveguide bend fabricated. This device component is useful to direct all fanout beams into a single direction at the end of waveguide in an optical H-tree system [7]. Experimental results confirm that a decently curved waveguide has a much lower loss when compared with 90° waveguide bend using a total internal reflection (TIR) mirror.

The waveguides under test were mounted on a precise six-axis prism coupling stage. A laser beam profile analyzer (Model Spiricon LBA-100A) was arranged to observe a light streak of the excited mode in the waveguide from the front. The output video signal from the camera was analyzed by the system to provide the waveguide propagation loss. There are two ways to sample the light intensity of the streak for loss measurement using a video camera, i.e., longitudinal and transverse scan samplings. The peak intensity variations along the streak can be ascertained by scanning along the propagation direction, and the loss value can be directly acquired from the longitudinal change. However, this one-dimensional (1-D) scanning applies only to the straight guides; also, setting the sampling line along the streak requires precise adjustment. Hence we scan transversely to the light streak. Repeating the same procedure along the streak, we can obtain two-dimensional (2-D) information of the intensity distribution. Repeating the integration of the data along each sampling line, we obtain the longitudinal variation of the mode intensity in the waveguide as shown by the dots in Fig. 4. The solid lines are the least mean-square fits to a decreasing exponential, the slope of which yields the power loss coefficient. The propagation loss of the TE fundamental mode of the channel waveguide is 0.21 dB/cm at 850 nm and 0.48 dB/cm at 632.8 nm.

III. Thin-Film Waveguide Couplers

To efficiently couple optical signals from VCSEL's to polymer waveguides and then from waveguides to photodetectors, two types of waveguide couplers are investigated. They are tilted grating couplers and 45° waveguide coupling mirrors. There are a large number of publications in grating design [8]–[12]. However, the surface-normal 1-to-1 coupling scenario in optical waveguides has not been carefully investigated so far. We are interested in a tilted grating profile in a planar structure within a thin waveguide layer upon which other microlithographically defined electrical interconnection layers can be built. Such a configuration requires the insertion of optical interconnect layer to be planarized. The tilted grating profile greatly

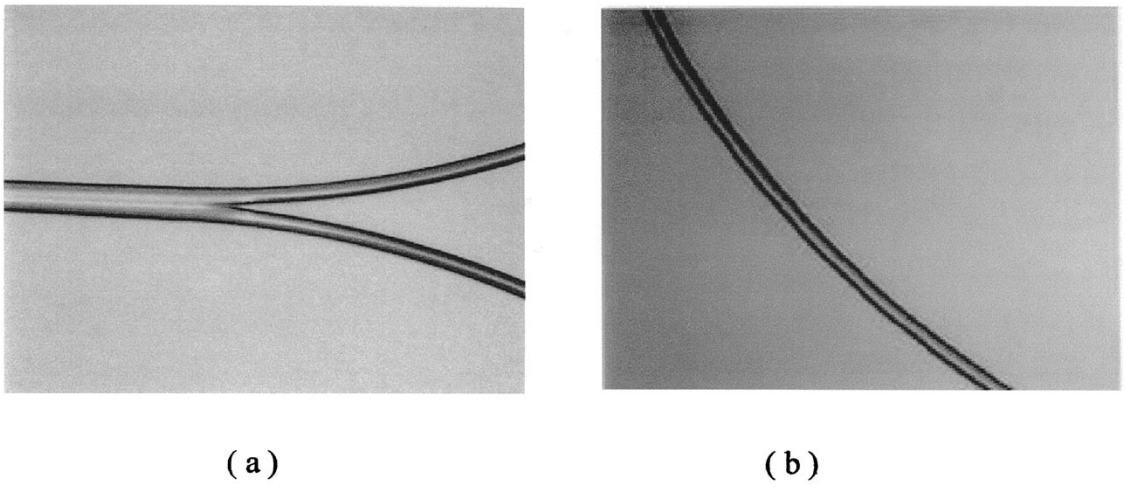

Fig. 3. (a) photograph of 1-to-2 3-dB waveguide splitter and (b) a 90° waveguide bend.

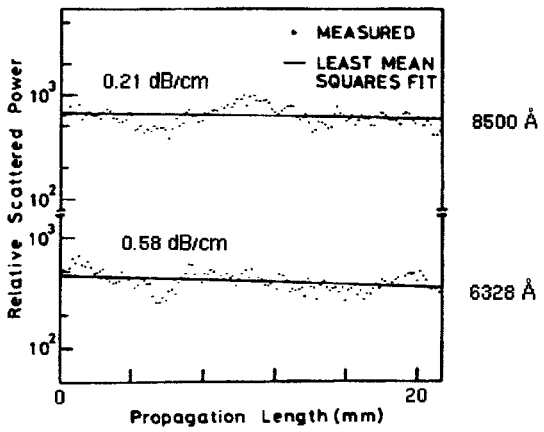

Fig. 4. Loss measurement of the polyimide waveguide at (a) 850 nm and (b) 632.8 nm.

enhances the coupling efficiency in the desired direction. The phenomenon of grating-coupled radiation is widely used in guided-wave optical interconnects. Very often coupling in a specific direction is required. To achieve this unidirectional coupling, the tilted grating profile is selected as a high-efficiency coupler. A very important aspect of manufacturing of such a coupler is the tolerance interval of the profile parameters, such as the tooth height, the width, and the tilt angle.

Consider the structure of the waveguide coupler shown in Fig. 1 where the guided-wave optical interconnection layer (layer 4) is sandwiched among other six electrical interconnection layers on a PC board. For a transverse electric (TE) guided mode, the E-field is along the z-direction and satisfies

$$\frac{\partial^2 E_z}{\partial x^2} + \frac{\partial^2 E_z}{\partial y^2} + k^2(x, y)E_z = 0 \qquad (1)$$

where the time dependence $\exp(-i\omega t)$ has been omitted, $k(x, y)$ is the wave vector with $k(x, y) = k_0 n(x, y)$, $k_0 = (2\pi/\lambda)$, λ is the free space wavelength, and $n(x, y)$ is the refractive index. We can express field E_z as an Floquet's infinite summation of partial waves

$$E_z(x, y) = \sum_{m=-\infty}^{\infty} E_m(y) \exp(i\alpha_m x) \qquad (2)$$

where $\alpha_m = \alpha_0 + m(2\pi/\Lambda)$ and Λ is the grating period; α_0 is a phase constant.

We have employed an accurate analytical technique to calculate radiation from tilted diffraction grating and determine optimum grating microstructures to maximize coupling in one diffraction order. To provide effective free-space-to-waveguide and waveguide-to-free-space conversions, the microstructure of the surface-normal grating coupler shall be tilted to furnish the needed phase-matching condition at one waveguide propagating direction rather than two. The tilt angle of the grating corrugation determines the vertical component of the grating $\boldsymbol{K}$ vector to provide the required phase-matching condition both horizontally and vertically. The polyimide waveguide can be fabricated on different substrates such as PC board, Si, glass, and others by spin coating. To fabricate polyimide waveguides, an A600 primer layer was spin-coated first on the substrate with a spin speed of 5000 rpm and prebaked at 90 °C for 60 s. The Amoco polyimide 9120D was then spin-coated with a speed of 2000 rpm. A final curing at 260 °C in nitrogen atmosphere was carried out for more than three hours. Typical thickness of the waveguide was 7 μm. The planar waveguide has also been successfully fabricated on Si substrate by inserting a high index polyimide layer ($n = 1.56$–1.76) between the 9020D cladding layers.

To form the tilted grating pattern on the polyimide waveguide, we used a reactive ion etching (RIE) process with a low oxygen pressure of 2 KPa to transfer the grating pattern on aluminum layer to the polyimide layer. In order to get the tilted profile, a Faraday cage was used [13]. The final step was to remove the aluminum mask by another step of RIE process. Microstructures of the tilted grating having a periodicity varying from 0.5 to 3 μm have been fabricated. Fig. 5(a)

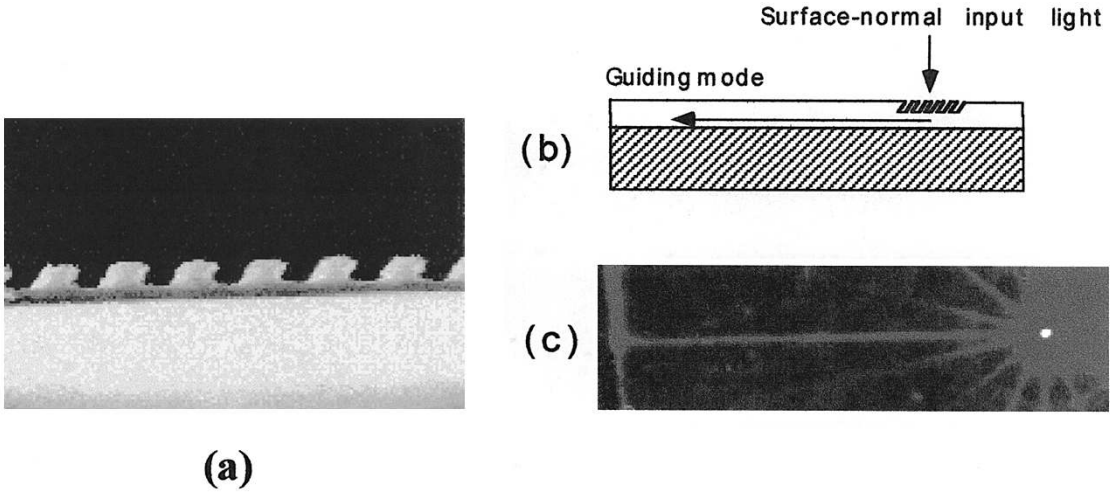

Fig. 5. (a) SEM picture of a tilted grating which has a tilted angle of 32°. Grating periods from 0.5 to 3 μm have been successfully fabricated with an aspect ratio of 1.1. (b) The schematic of coupling a surface-normal input light into waveguide using the tilted grating. (c) The experimental photograph of coupling a surface-normal input 632.8 nm He–Ne light into the polyimide waveguide.

shows one of many gratings from a scanning electron microscope (SEM) picture.

A test waveguide sample with a tilted grating as the surface-normal input coupler was built using 632.8 nm as the operating wavelength. The schematic of coupling a surface-normal input light into a waveguide using the device fabricated is shown in Fig. 5(b), together with an experimental photograph in Fig. 5(c). The coupling to the planar waveguide with the unidirectional propagation can be clearly observed with a measured efficiency of 35%. Note that the index difference between the guiding layer and the substrate layer is less than 0.03 for the device shown in Fig. 5. Theoretical results show that the index difference between the guiding and the cladding layers plays an important role in enhancing the coupling efficiency.

The second method of waveguide coupling is through the total internal reflection. Such a waveguide coupler is much less wavelength sensitive and can be easily manufactured using reactive ion etching, and a similar procedure for fabricating polyimide-based channel waveguides. The input coupling efficiency of micromirror coupler is higher than 90% when a profile-matched VCSEL is employed [14]. The output coupling efficiency is almost 100% due to the termination of waveguiding path. A linear channel waveguide array with 12 parallel channels (50 $\times$ 10 μm^2) made with two oppositely faced 45° TIR waveguide couplers is further illustrated in Fig. 6, where three out of the twelve channels are clearly shown with the 45° TIR waveguide couplers. Note that the channel to channel separation is engineered to be 250 μm due to the consideration of fiber array coupling.

To facilitate the system integration, the surface-normally coupled optical beams at 850 nm coming out of the 45° waveguide coupler are studied. The output profiles from one of the 45° microcouplers are shown in Fig. 7(a)–(c). These figures correspond to $z = 100$ μm, 1 mm, and 5 mm, respectively (z is the distance from upper surface of the coupler to the point of observation). The output coupling efficiency of this 45° microcoupler is nearly 100%. The half width at half maximum (HWHM) of the output profile at the microcoupler is about 60 μm, which is comparable to the active region of a silicon-based photodetector having a bandwidth of several gigahertz [15]. If the photodetectors are mounted close to the microcouplers, then most of the light can reach the photodetectors and thus the coupler-to-detector coupling efficiency can be very high.

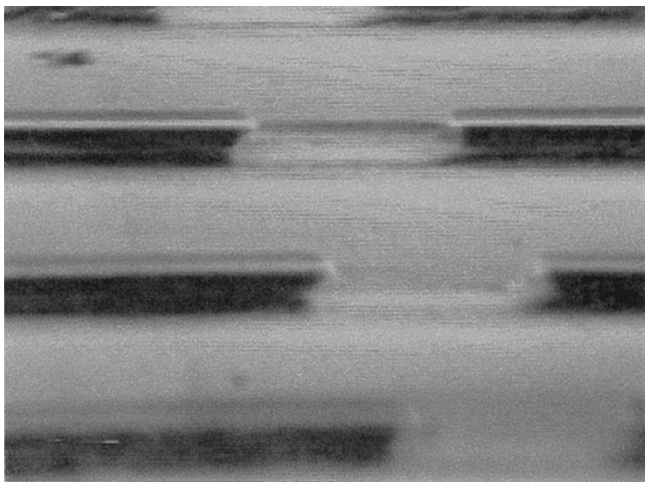

Fig. 6. SEM picture of a section of linear polyimide channel waveguide array with two oppositely faced 45° waveguide couplers, which function as input and output couplers, respectively. The channel waveguide has a cross section of 50 μm (width) $\times$ 10 μm (depth) and the channel to channel separation is 250 μm equivalent to the optical fiber array spacing.

The output profile from the 45° microcoupler can be determined using diffraction theory. We use Fresnel approximation [16], [17] to get the near-field distribution $U(x, y)$, which is given by

$$U(x, y) = \frac{\exp(jkz)}{jz\lambda} \int_{-\infty}^{\infty} U(\xi, \eta) \cdot \exp\left\{ \left(j \frac{kz}{2z} [(x-\xi)^2 + (y-\eta)^2] \right\} d\xi\, d\eta$$

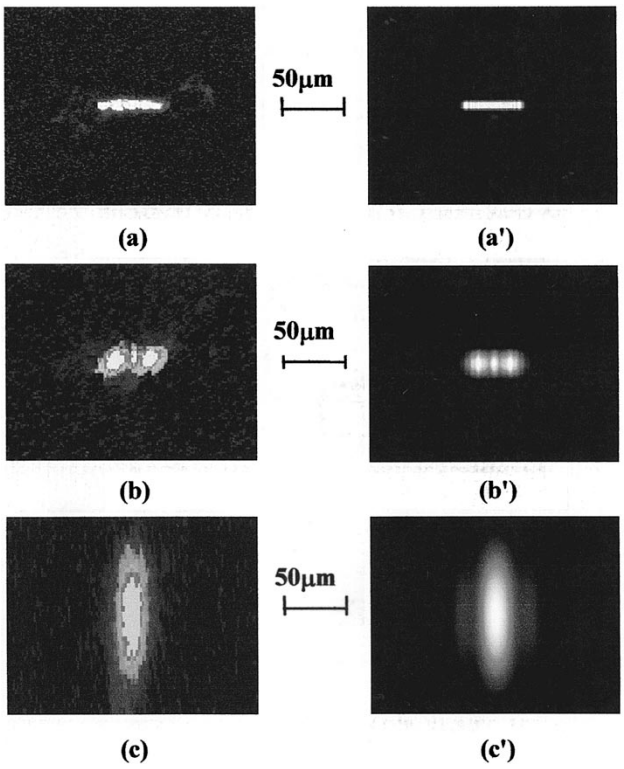

Fig. 7. The output profiles from the 45° surface-normal microcoupler (a) $z = 100$ μm (experiment); (b) $z = 1$ mm (experiment); (c) $z = 5$ mm (experiment); (a′) $z = 100$ μm (theory); (b′) $z = 1$ mm (theory); and (c′) $z = 5$ mm (theory).

where $U(\xi, \eta)$ is the complex amplitude of the excitation at point (ξ, η) on the 45° microcoupler. $U(x, y)$ is the complex amplitude of the observed field at point (x, y), and k the magnitude of wave vector and z the distance from the upper surface of the 45° microcoupler to observation point. The theoretical output profiles at $z = 100$ μm, 1 mm, and 5 mm from the 45° microcoupler are shown in Fig. 7(a′)–(c′), respectively. In this calculation, the input to the microcoupler was assumed to be the fundamental mode of the waveguide. It turned out that most of the energy was in fundamental mode in our case. There is a good agreement between the theoretically simulated and experimentally observed output profiles.

IV. Integration of Thin-Film Transmitters and Receivers

The operating wavelength is chosen to be 850 nm. High-performance VCSEL's are available with an output wavelength of 850 nm [18]. These laser devices, compared to conventional edge-emitting lasers, offer a very low threshold current with much less temperature sensitivity, moderate optical power (few mW), very high direct modulation bandwidth (>14 GHz), wide operating temperature range (−55 °C to +125 °C), and ease of packaging in an array configuration due to the unique surface-normal output nature. To provide a high coupling efficiency using the proposed waveguide couplers, the control of the emitting aperture and of the wavelength are pivotal, which makes VCSEL's the best choice due to the large separation of the adjacent longitudinal modes implied by the short cavity length. To provide the required fanouts with a bit error rate of 10^{-9} at the required speed, a VCSEL with enough modulated power is needed to accommodate all losses including the −3-dB power margin. Planar configuration of VCSEL's allows these devices to be fabricated and wafer-scale tested with conventional microelectronics manufacturing processes. The unique surface-normal emitting nature of the device allows us to use exactly the same packaging scheme for coupling light from VCSEL into waveguide as that used for coupling light from waveguide into photodetector. In order to individually address each VCSEL in an array, each anode was contacted separately and attached to individual bonding pads upon which a synchronized driving signal shall be applied. The important aspects of the VCSEL for fully embedded-type board-level optical interconnects application are its very thin laser cavity, typically less than 10 μm, and surface-normal emitting characteristic. If the substrate of the VCSEL was removed, very thin VCSEL enables the formation of a fully embedded optical interconnection, as depicted in Fig. 1. However, VCSEL in this embedded scheme was surrounded with a thermal insulator such as polymer; therefore, generated heat builds up within the embedded layer. This necessitates consideration of efficient heat-removal methods. Intrinsically, heat generated inside of the thin VCSEL will be more rapidly transported to the surfaces of VCSEL than that of thick VCSEL. A forced heat removal method using via and thermoelectric cooler (TEC) can be the best choice for effective cooling. Via, which feeds electrical current to VCSEL, can be used as a heat conduction path, simultaneously. TEC attached on a metal pad of the top layer of a printed circuit board effectively will cool down the temperature of the via.

To demonstrate a parallel channel interconnection, an 850-nm linear VCSEL array with 12 independently addressable lasers with 250-μm separation is employed. The threshold current and slope efficiency is measured to be 7 mA and 0.5, respectively. To incorporate the VCSEL array onto the fully embedded architecture, the VCSEL array has to be thin enough to build such a 3-D structure. There are two methods to make thin-film VCSEL: mechanical polishing and epitaxial liftoff [19]–[21]. The substrate removal by using the epitaxial liftoff is based on extremely selective etching ($>10^9$) of AlAs in diluted hydrofluoric acid. The epitaxial liftoff method has advantages of reproducibility and mass producibility. To adapt epitaxial lift-off method, VCSEL devices should be fabricated on top of the AlAs sacrificial layer, which is located between the bottom distributed Bragg reflector and GaAs substrate [19]–[21]. A mechanically polished thin VCSEL array is shown in Fig. 8(a) and (b). Fig. 8(a) shows a section of the 12-channel VCSEL's, and Fig. 8(b) shows the SEM picture of the mechanically polished thin VCSEL array where the thickness of the GaAs is measured to be 42 μm. An n-ohmic contact was fabricated on the polished side using Cr(40 nm)/Au(200 nm) and annealed at 350 °C for 20 s.

Output laser power and current versus voltage characteristics of the VCSEL before and after polishing down to 42-μm

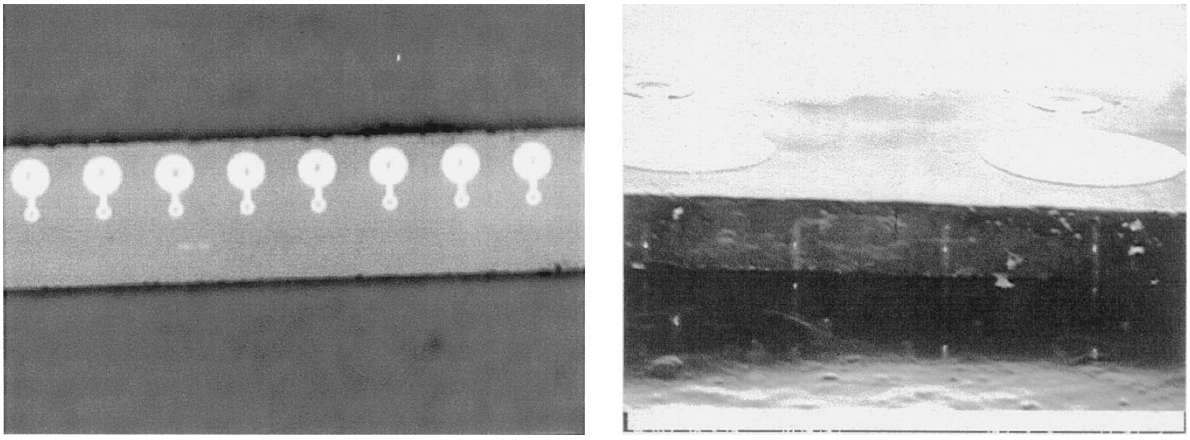

(a) (b)

Fig. 8. An SEM picture of a section of a linear thin film VCSEL array with 12 elements. The thickness of the substrate is 42 μm. The emitting aperture is 15 μm. Two individually addressable VCSEL's are shown.

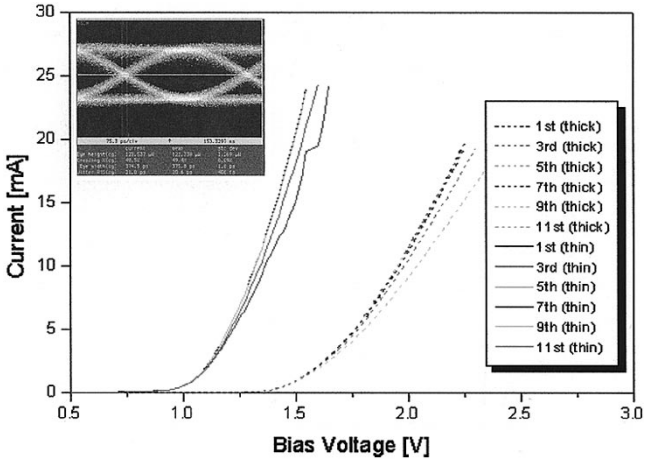

Fig. 9. The I–V curves of the linear array. Six of the twelve elements are shown. The improvement of the threshold currents after polishing is indicated.

thickness are measured, and the result is shown in Fig. 9. The VCSEL array was mounted on gold-coated substrate using an InGa eutectic alloy. Threshold current and threshold bias voltage are measured before thinning to be 5.8 mA and 1.7 V, respectively, and those of after thinning to be 6.0 mA and 1.2 V, respectively. After polishing to its final thickness, there is no significant change in optoelectrical characteristics. The L–I curves showed that there was no kink. The current versus voltage (I–V) curve showed that the series resistance after thinning (200 Ω) was smaller than that of original (300 Ω) at threshold voltages. It is obvious because the series resistance of the VCSEL is reduced. A speed measurement has also been conducted using an RF probe stage and the eye diagram of the VCSEL operating at 2 Gbit/s. The result is displayed in the inset of Fig. 9. It is to be noted that the fully integrated version of the embedded optical interconnection using such a VCSEL array is to be addressed using electrical vias from the surface of the PC board.

Advanced optical and optoelectronic systems for high-speed communications require complex combinations of components for generating, amplifying, and detecting optical signals. High-performance receivers require both high-quality transistors and photodetectors. There are three types of photodetectors. They are p-i-n photodiode, metal–semiconductor–metal (MSM) photodetector, and avalanche photodetector (APD). Numerous high-performance monolithic Si and GaAs receivers have been demonstrated, with the integration of MSM detector and field-effect transistors (FET's). In the context of board-level optical interconnect applications, a thin-film MSM photodetector is the most appropriate because it can provide a very high demodulation speed due to the fast transit time of electron and hole pairs and is compatible with Si CMOS fabrication procedure [22]–[24].

We present a thin-film silicon MSM photodetector that can be directly integrated onto the system architecture shown in Fig. 1. The finished photodetector is the MSM on a 10-μm -thick silicon wafer with a rough back surface. High speed is achieved because the thin film ensures that the photogenerated electron/hole pairs are only created in the high field region. Also the rough back surface scatters the light and traps it inside the thin film to compensate for otherwise low quantum efficiency [25].

The devices were fabricated on an n-type, (100)-orientation silicon wafer. The resistivity of the wafer is 10 Ω-cm, which indicate that the doping level is about 10^{15}. The 1000 Å SiO_2 was deposited by plasma-enhanced chemical-vapor deposition (PECVD). The silicon dioxide layer served to isolate optically inactive metallization areas and reduce junction capacitance. The inter-digitated fingers were patterned. Then the silicon dioxide of the pattern was wet etched accordingly, and the 500-Å gold layer was uniformly deposited. The I–V characteristic is measured (not shown). Fig. 10(a) shows the 10-μm-thick silicon film with a fabricated MSM photodetector array having 2-μm fine lines of the electrode pattern illustrated in Fig. 10(b). The spacing between fingers and the finger width are all 2 μm, resulting in a relative photosensitive area of 50%. The experimental results conclude that the adjacent metal/semiconductor/metal interfaces are two Shottky barriers, which

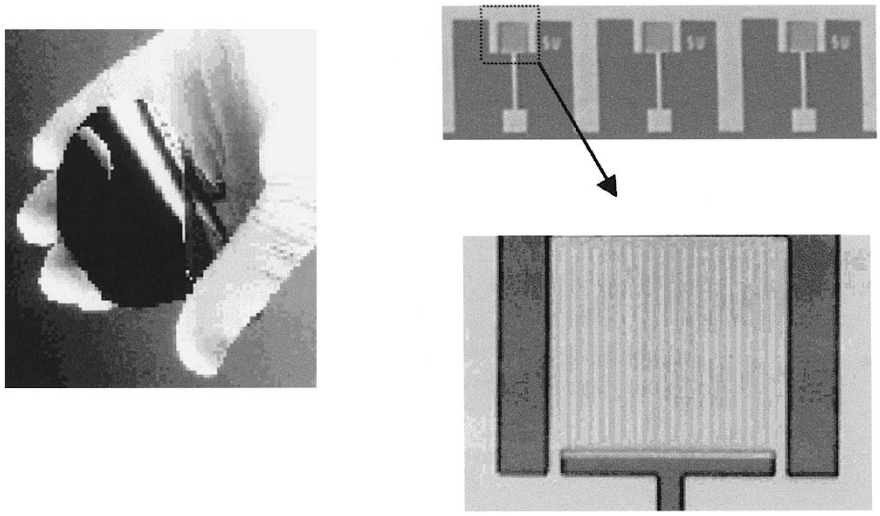

(a) (b)

Fig. 10. (a) A silicon wafer with 10 μm thickness upon which MSM photodetector is built and (b) a section of a linear array of Si-based MSM photodetector.

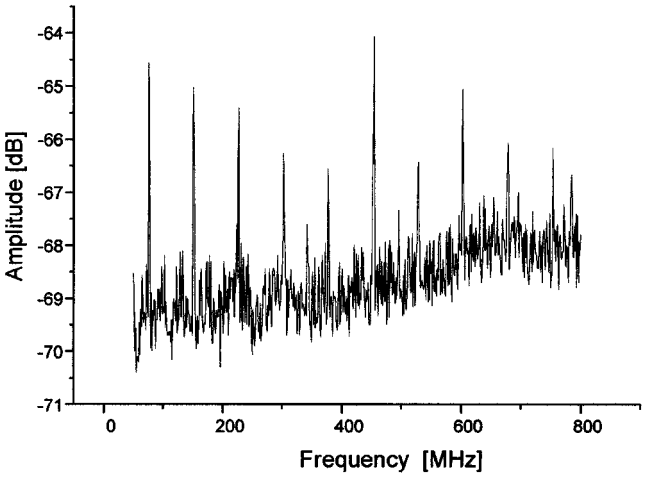

Fig. 11. Speed measurement of a bulk Si MSM photodetector. 800 MHz is shown. The polished sample shall have a speed well above 2 GHz due to the much shorter transit time of electron/hole pairs.

serve as two back-to-back diodes. When a bias is applied across the fingers, one junction becomes reverse biased, while the other one becomes forward biased. Electron-hole pairs are photo-generated within the bulk region of the device when illuminated with an 850-nm VCSEL beam. The application of a bias to the metallic fingers creates an electric field within the underlying semiconductor that acts to sweep the photo-generated carriers out of the device. The dark current was measured by using an HP semiconductor parameter analyzer. The dark current at 5-V bias voltage is 52 nA. The low dark current ensures the high signal-to-noise ratio.

The speed was measured using a pulse laser working at 850-nm band. The electrical signal was picked out by a high-speed probe and fed into spectrum analyzer. The bandwidth measurement up to 800 MHz is provided, see Fig. 11. The key conception of this design is that the thin film dramatically increases the electrical field inside the silicon. Therefore, the saturation velocity of holes, the predominant restrictive parameter on increasing the speed of photodetector, will be increased. Because the absorption length is 9 μm, when the silicon wafer is thinned down to around 3 μm, the enhancement of the speed will be above 2.5 GHz, which is around three times the speed of photodetector on bulk silicon. The bandwidth does not reach 2.5 GHz because the wafer has not been thinned down around 3–5 μm. The long absorption length combined with the weak electrical field down to the silicon surface result in the long life time of the photogenerated carriers.

V. Optical Clock Signal Distribution

For a multiprocessor computer system, such as a Cray T-90 supercomputer, it is difficult to obtain high-speed (>500 MHz) synchronous clock distribution using electrical interconnections due to large fanouts (48 $\times$ 2) and long interconnection lengths (>15 cm) [27]–[31]. A fanout chip is required to provide the massive electrical fanout. The synchronous global clock signal distribution is highly desirable to simplify the architecture and enable a higher speed performance. High-speed, large-area massive fanout optoelectronic interconnects may overcome many of the problems associated with electrical interconnects in this interconnection scenario [27]–[35]. An array of a novel optical interconnect architecture has been proposed and then demonstrated by earlier researchers [35]–[37], which may partially satisfy the above requirements for a massive clock signal distribution in intraboard and interboard hierarchies.

In this section, we report the development of a guided-wave optoelectronic interconnect network for optical clock signal distribution for a board-level multiprocessor system. For comparison, the electrical interconnect network of the clock signal distribution for Cray T-90 supercomputer at the board level currently employed and the corresponding implementation of optical interconnection are shown in Fig. 12(a) and (b), respectively. Fig. 12(a) shows the existing 500-MHz 1-to-48 clock signal distribution (one

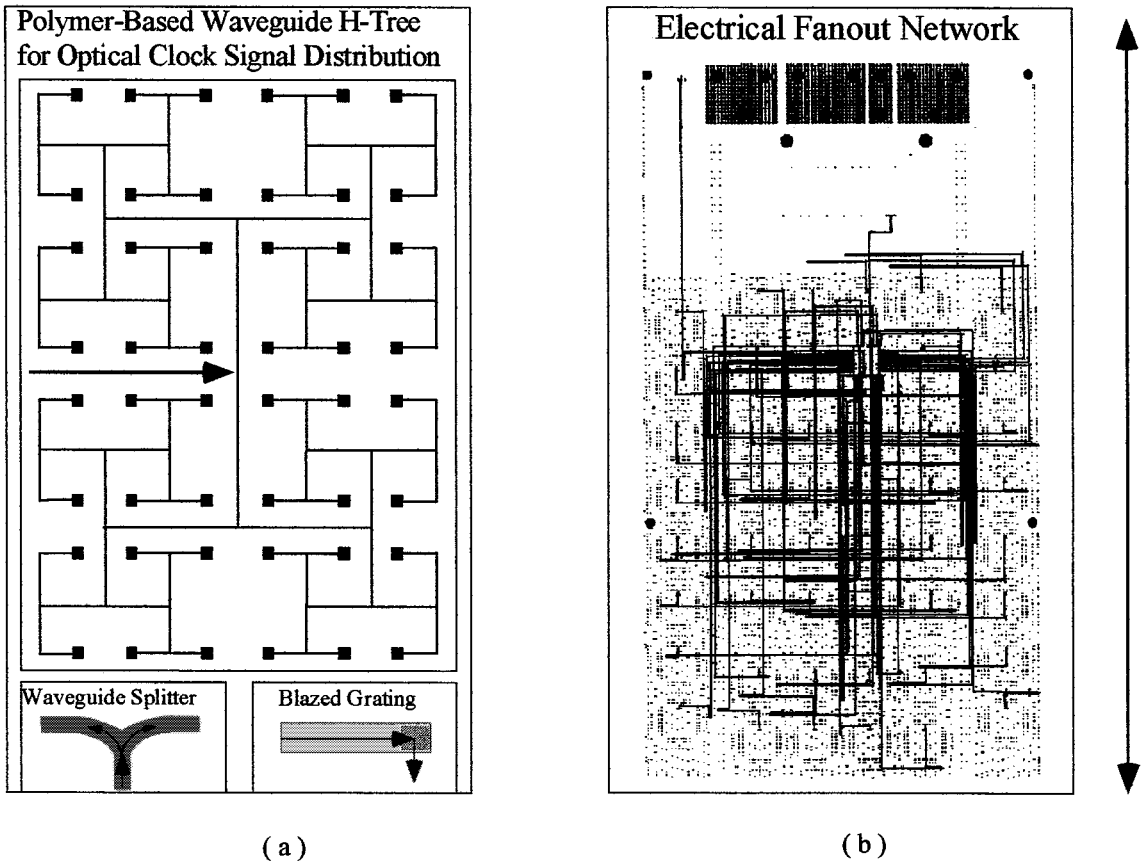

Fig. 12. Schematic diagrams of massive clock signal distribution networks using (a) an optical waveguide H-tree and (b) an electrical clock signal transmission line network that forms one of the 52 layers of Cray T-90 Supercomputer board. The holes indicate the feed-through marks of the on-board three-dimensional interconnections.

side) realized in one of the 52 vertically integrated layers within the Cray-T-90 supercomputer board. To further upgrade the clock speed, an appropriate optical interconnect scheme shown in Fig. 12(b) has to be incorporated to minimize electrical interconnection induced unwanted effects. An integrated board-level optoelectronic interconnection layer is constructed using the building blocks mentioned in this paper. Such a guided-wave optoelectronic interconnect network is to be inserted into the Cray supercomputer boards to become an additional optical interconnection layer among many other electrical interconnection layers. As a result, the future supercomputer system may have a clock speed more than ten times higher than current systems.

Our approach is to construct an additional optoelectronic interconnection layer (OIL) for the high-speed optical clock signal distribution using polymer-based guided-wave devices. The selection of guided-wave approach is mainly based on the system alignment and reliability concerns [38]. During the course of research, Si CMOS process compatibility and planarization of the OIL are the two major technical concerns. As shown in Fig. 12(a), a polymer-based waveguide H-tree system is employed to replace the existing electrical fanout interconnect network shown in Fig. 12(b). The optical clock signal delivered by an optical fiber is coupled into the OIL using an input surface-normal waveguide coupler and distributed through out the board by the polymer-based channel waveguide network. The distributed optical clock signal at each fanout end will be coupled into a corresponding photodetector by an output surface-normal grating coupler. A 6-GHz optical clock rate was demonstrated previously using such a waveguide H-tree structure.

The building blocks required to facilitate such an optical H-tree system [Fig. 12(a)] include high-performance low-loss polymer-based channel waveguides, waveguide couplers, 1-to-2 3-dB waveguide splitters, and 90° curved waveguide bends. These components allow the formation of a waveguide H-tree for the required optical clock signal distribution, where all the optical paths have the same length to minimize the clock skew problem. The employment of optical channel waveguides and surface-normal waveguide couplers provides a compact, mechanically reliable system. Due to the nature of massive fanouts (48) over a large area, the waveguide propagation loss must be minimized while the waveguide grating coupling efficiency has to be maximized. These two factors are very important to ensure enough optical power at the end of photodetectors for high-speed operation. While fiber optics technology has been successfully implemented among cabinets as replacements for coaxial cable point-to-point link, its application inside a cabinet on the board-level system is severely limited due to the bulkiness of fibers, fiber connectors, and significant labor and cost involved in parallelism of the interconnects. Recent achievements in plastic fiber-based optical inter-

connects have demonstrated an optical interconnect from a centralized light source to a one-to-many direct fanouts within one board. Several Gbit/s optical signal transmission has been demonstrated experimentally [39]–[41]. While having the advantages of low loss and easy implementation of the optical layer, this type of interconnect has an intrinsic drawback in intraboard optical interconnection. The alignments of laser-to-fiber and fiber-to-detector are difficult to achieve. In the context of optical clock signal distribution, alignment of 48 plastic fibers to 48 independently addressed photodetectors cannot be easily achieved. Polymer optical waveguide technology, on the other hand, is particularly suitable for intraboard interconnects applications for its large area waveguide formation, and each lithography layer is precisely aligned. It can be viewed as an optical equivalent of electrical printed wiring board technology in which the fabrication cost is independent of the interconnect functionality and complexity. In order to take the advantages of the polymer waveguides, we must be capable of implementing optoelectronic devices such as laser diodes and photodetectors in the same PC board package. The polymer waveguides can be fabricated, integrated, and packaged into the board with the fully embedded architecture shown in Fig. 1; the insertion of optical interconnects becomes an acceptable approach to upgrade the microelectronics-based high-performance computers.

An optical H-tree fanout network based on polyimide channel waveguides was fabricated for optical clock signal distribution in a Cray multiprocessor supercomputer board. The original design of the Cray-T-90 supercomputer was based on an external laser diode modulating at 500 MHz, which went though a 1-to-32 waveguide star coupler to provide a system clock to 32 different boards of the supercomputer. At the edge of each board, the optical clock was converted to an electrical clock signal. The 1-to-48 fanouts of all 32 boards were realized through delay-equalized electrical transmission lines. The communication distance of these clock lines within each board is as long as 32.6 cm, which makes the further upgrade of the clock speed to gigahertz level unrealistic. To release such a bottleneck, we demonstrate an optical clock signal distribution using the building blocks mentioned in the previous sections. Polyimide waveguides are employed as the physical layer to bridge the system clock optically to the chip level. As a result, the distance of electrical interconnection to realize the system clock signal distribution at the gigahertz level will be minimized at the chip level instead of board level. The H-tree structure is selected to equalize the propagation delays of all 48 fanouts. Due to the relatively short interconnection distance, the waveguide is multimode with a cross section 50 μm wide and 10 μm deep. The horizontal dimension of the waveguide is to match the 50-μm multimode glass fiber, and the vertical dimension can be matched with a three-dimensional tapered waveguide [38]. Both tilted grating couplers and 45° TIR mirror couplers are fabricated to efficiently couple light in and out of the H-tree waveguide structure. The 45° TIR mirror provides a better coupling efficiency and a shorter interaction length to fulfill such a coupling. Fig. 13(a) shows the broadcasting of the optical signal through the H-tree structure at 632.8 nm. Forty-eight

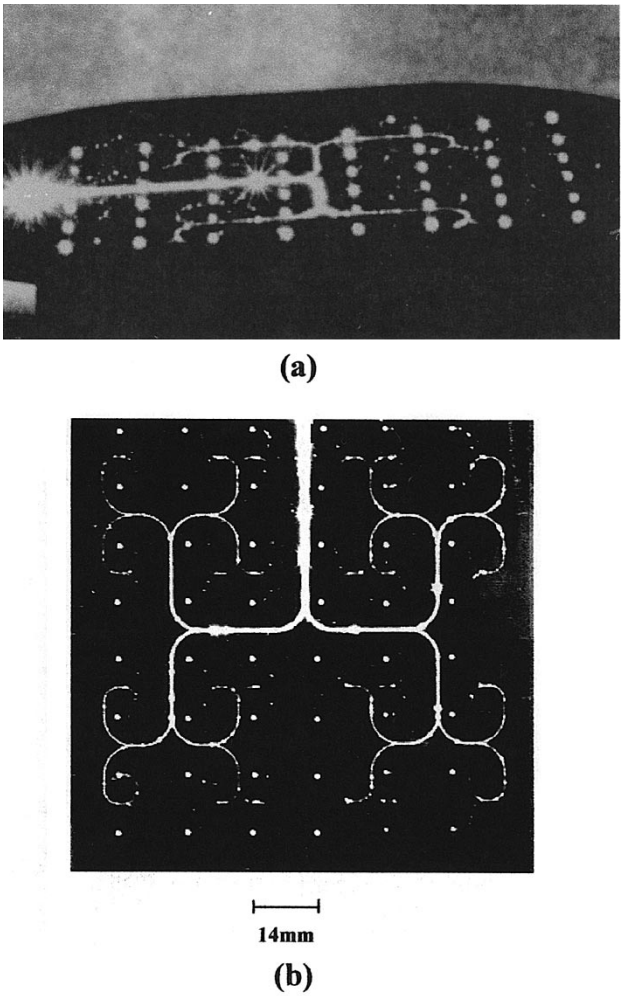

Fig. 13. (a) Optical clock signal distribution using 632.8 nm as the input laser beam. The 48 outputs are realized using 45° TIR mirrors. (b) Board level clock signal distribution using 850 nm VCSEL with the same output coupling mechanism as that of 13(a).

well-defined light spots are coming out surface-normally. Fig. 13(b) is using a fabricated 1-to-48 H-tree waveguide structure operating at 850 nm. All 48 surface-normal fanouts are provided through 45° TIR waveguide mirrors. Based on the loss measurement, a VCSEL with enough modulated power is needed to compensate −2-dB coupling loss, −6-dB waveguide propagation loss, −17-dB fanout loss, −3-dB bending loss, and −3-dB power margin. The employment of the H-tree waveguide structure is to equalize the propagation delays of different locations where Si-based clock detectors were located. We are in the process of investigating the feasibility of further reducing the bending losses by using curved waveguides, which have lower bending losses than the present structure.

To ensure the polyimide waveguide material can function as the physical layers of optical bus and also the interlayer dielectric, a multilayer test structure is made. Three electrical interconnection layers and three metal layers are formed. Each polyimide layer is 37 μm thick, and metalized vias are formed to provide vertical interconnect involving different layers. A cutaway perspective of the MCM structure and a micrograph of the MCM cross-section showing a multilayer

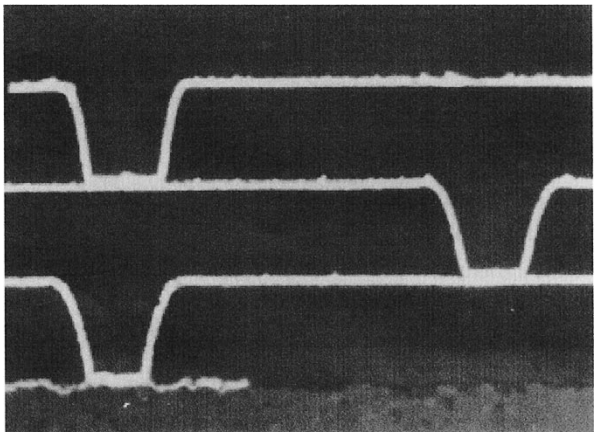

Fig. 14. Electrical vias showing vertical integration involving multiple polyimide layers.

polyimide thin-film dielectrics with metalized electrical vias is shown in Fig. 14 where the planarized electrical interconnection is shown in white. The bottom layer is the PC board.

VI. Polymer Waveguide-Based Optical Bus Structure

Unlike the optical interconnect, the electrical interconnect on the board level has two serious problems that significantly limit the data transfer speed. They are signal propagation time delay and skew between parallel bus links. These problems become more stringent when the linear dimension of a board increases.

The propagation time does not affect the maximum data rate of an uncompelled asynchronous block transfer [such as the source-synchronous block transfer (SSBLT), which is proposed for addition to the VME bus standard]. However, it does limit other types of bus transactions: address transfers, handshake single-word transfers, bus contention, and so on. Estimates have been made by Sweazey [42] of the sustained throughput, i.e., the data transfer rate averaged over a time that is long compared to the duration of a single transaction. Assuming that bus overhead is 200 ns per read and 100 ns per write operation, and assuming reads outnumber writes by 2 to 1, Sweazey calculated the sustained throughput as a function of block transfer speed (burst speed) and of the number of bytes per transfer. For 64-byte transfers, the calculated sustained throughput is 196 MB/s for a burst rate of 400 MB/s and 384 MB/s for infinitely rapid block transfers. The propagation speed for the electronic bus is at present greatest for backplane-transceiver logic (BTL) backplanes such as FutureBus: about 0.18 c (c is the speed of light in vacuum), giving a 15-ns round-trip time for a 40-cm backplane. This cannot decrease by much, since it is based on the extremely low driver capacitance of 5 pf/driver provided by BTL.

Uncompelled block transfers are limited by bus line skew. The principal cause of this is speed variations (time jitter) between transceiver chips. This jitter is at least 5 ns, even for a well-designed set of transceivers. This means that there will be a total skew between data lines and strobes of up to 20 ns from transmission to receiver latching. In addition, there may be skew in the transmission lines themselves, due to unequal capacitive loading, unequal distances to ac grounds, or for some other reason. (FutureBus transmission lines are purposely skewed to ensure that data arrive before strobe.) These skews limit the attainable transfer rate to 40 mega transfers/s or 160 MB/s for a 32-bit bus. Electronic bus lines are not typically terminated in a matched impedance, since this would require the drive currents to be too high. Therefore, the bus line will not settle until all end reflections have subsided (several round-trip times). By contrast, polymer bus lines may be terminated in antireflection coatings, suppressing end reflections and reducing settling time to zero.

A. Optical Equivalent for Electronic Bus Logic Design

Before discussing an optical backplane design in its entirety, we must present optical equivalents of necessary bus components, such as bidirectional transmission lines, stubs, transmitters, and receivers. Further, optical equivalents of line voltage, logic levels, and open-collector and tristate line driving and receiving must be derived. Once these issues are resolved, the way will be clear for defining an optical bus that is fully compatible with existing IEEE standardized bus protocol.

The optical equivalent of a PC board trace is a polymer-based optical waveguide. A very important consequence is the ability to provide modulation using VCSEL's and demodulation using photoreceivers for the same board where the polymer waveguide is located. An unloaded (no boards attached) PC board trace has a typical signal propagation speed on the order of 0.6 c. The speed drops to below 0.2 c for a fully loaded bus line. The polymer, which forms the optical waveguide, has an index of refraction $n \cong 1.5$. The optical signal propagation speed is $c/n \cong 0.67$ c, similar to that of the unloaded electronic bus line.

It is important to note, however, that there is no optical analog to driver capacitance from attached boards, which causes loading of electronic bus lines. Therefore, the optical signal speed retains the same high value regardless of the presence or absence of line drivers in the system. This means that the optical bus round-trip delay time will be lower by a factor of three than that of the electronic bus. A connection to an electronic bus line takes the form of a stub or tee junction in the PC board trace; usually, such a stub connects to a line transceiver. The optical equivalent of a stub is high-efficiency waveguide couplers, such as tilted gratings or 45° TIR waveguide mirrors, which allow light from a second waveguide to be coupled into the optical bus line, and low-efficiency coupling, which will be used to couple light out of the bus for detection. The key feature of the couplers is that while light is injected from the stub with high efficiency, light propagating in the bus line and passing the coupler is almost unaffected by it ($<1\%$ fan-out). This is not the case, however, for light propagating in the other direction, which suffers high losses at the coupler.

Because of this, an optical waveguide with stubs attached is necessarily unidirectional. The optical equivalent of an electronic bus line thus involves two parallel optical waveguides, each carrying light in the opposite direction as depicted in Fig. 15. Optical waveguide signals can be

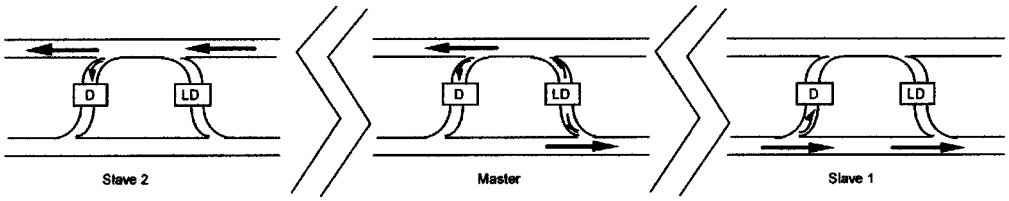

Fig. 15. The optical equivalent of a bidirectional electronic bus line driven by open-collector drivers (TIR waveguide mirror coupling is not shown). Communication between one master (e.g., processor) and two slaves (e.g., memories) is clearly indicated (boards not shown). Commands from the master to slaves 1 and 2 are carried out using the bottom and the top polymer buslines, respectively. In this specific scenario, the Master is broadcasting signals that are received by Slaves 1 and 2, and the high power margin of the operation is preserved.

detected at much lower levels than the level of transmission. For instance, a VCSEL can easily provide a 5-mW modulated power, while a photodetector (e.g., a p-i-n diode) can detect a 5-μW signal at 5 Gbit/s. This implies high fanout capability, i.e., many receivers can be connected using low-efficiency couplings to a bus line driven by one transmitter. Fig. 15 shows the optical equivalent of a single bidirectional electronic bus line. The drive current provided by each electronic transceiver powers the corresponding laser diode, whose output is split and injected into both waveguides. Each photodiode detects light from either waveguide, since the low-efficiency couplings lead to waveguide segments, which are merged with a unidirectional coupler. Each photodiode current powers the corresponding electronic receiver.

The scheme in Fig. 15 may be considered fully equivalent to an electronic bus line driven by open-collector drivers, terminated in pullup resistors, if the following identification is made:

- the state in which no light is present on either waveguide (no laser diode is operating) corresponds to the unasserted electronic line, which is pulled high by the pullup resistors;
- the state in which there is light in both waveguides (one or more laser diodes are operating) corresponds to the asserted (low-level) electronic line.

Note that there is no optical effect corresponding to the wire-OR glitch. When two diodes are on, and one turns off, every detector continues to receive light from the other as long as it remains on. This is because the optical powers from two diodes simply add in the waveguide; any detected nonzero power (above a characteristic noise threshold) corresponds to the asserted line state.

The analog to resistive transmission-line termination is treatment of the ends of the optical waveguides on a PC board so that the reflected power is zero. This is done by implementing an antireflection coating or by fabricating the waveguide ends at the Brewster angle, with an absorptive beam dump outside the waveguides. If this optical isolation is done, settling-time effects are removed. Note that the optical bus line just described has exactly two states: light present (low) and light absent (high). This suffices, as just described, to represent a two-state open-collector-driven line exactly. However, it is insufficient to represent a tristate-driven line: a tristate driver has an asserted-high state, which is distinguishable from the disconnected state. Where the tristate line must be exactly emulated, the corresponding optical bus line can consist of a pair of the lines just described, that is, four optical waveguides, with a separate laser diode and a separate photodiode for each pair; see Fig. 16. In this case, the state with no light in any waveguide represents the disconnected state (no device asserting) as before, while the state with light present in the top pair (for example) indicates the asserted-high state, and that with light in the lower pair the asserted-low state. Note that this scheme overrepresents the tristate line, as there is a fourth state, that with light in both pairs of waveguides. The optoelectronic circuit can be integrated into a fully embedded optical interconnection layer as shown in Fig. 1. Each bus line consists of two optical waveguides, one OIC per plug-in board, couplings and stub waveguides, and power and ground lines (metal traces) to power the OIC's.

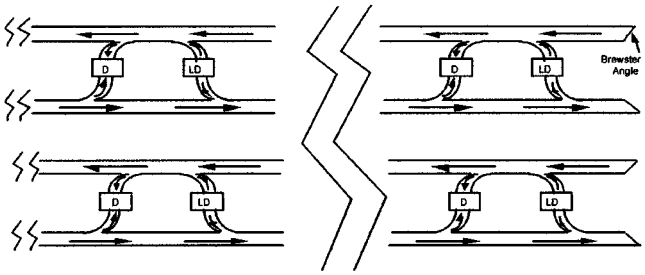

Optical Bus State	Tri-State Logic State
Light in Upper Waveguide Pair	Asserted High
Light in Lower Pair	Asserted Low
No Light	Disconnected (High Impedance)
Light in Both Pairs	No Equivalent

Fig. 16. The optical equivalent of a tristate bidirectional electronic bus line.

VII. Conclusion

In summary, a fully embedded board-level guided-wave optical interconnection is presented. All elements involved in providing high-speed optical communications within one board are demonstrated. These include a VCSEL, surface-normal waveguide couplers, a polyimide-based channel waveguide functioning as the physical layer of optical bus, and a photoreceiver. The driving electrical

signal to modulate the VCSEL and the demodulated signal received at the photoreceiver can be applied through electrical vias connecting to the surface of the PC board. By doing so, all the real estate of the PC board surface are occupied by electronics, and therefore one only observes the performance enhancement due to the employment of optical interconnection but does not worry about the interface problem between electronic and optoelectronic components unlike conventional approaches.

A 1-to-48 optical clock signal distribution network for Cray T-90 supercomputer is demonstrated. Further experimental results on a 12-channel linear array of thin-film Polyimide waveguides, VCSEL's (42 μm; can be made as thin as 8 μm), and silicon MSM photodetectors (10 μm) suitable for a fully embedded implementation are provided. Two types of waveguide couplers, titled gratings, and 45° TIR mirrors are fabricated within the polyimide waveguides. Thirty-five to near 100% coupling efficiencies are experimentally confirmed. A waveguide bus architecture is presented, which provides bidirectional broadcasting transmission of optical signals. Such a structure is equivalent to such IEEE standardized bus protocols as VME bus and FutureBus.

REFERENCES

[1] D. P. Seraphim and D. E. Barr, "Interconnect and packaging technology in the 90's," in *Proc. SPIE 1390*, 1990, pp. 39–54.

[2] R. O. C. Neugerbauer, R. A. Fillion, and T. R. Haller, "Multichip module designs for high performance applications," in *Multichip Modules, Compendium of 1989 Papers*: International Electronic Packaging Society, 1989, pp. 149–163.

[3] R. Haveman, "Scaling and integration challenges for Cu/low k dielectrics," in *Proc. Workshop Processing for ULSI: Transistors to Interconnects*, Austin, TX, Apr. 22, 1999.

[4] M. R. Feldman, "Holographic optical interconnects for multichip modules," in *Proc. SPIE*, vol. 1390, 1990, pp. 427–433.

[5] M. Feldman, I. Turlik, and G. M. Adema, "Microelectronic module having optical and electrical interconnects," U.S. Patent, 5 638 469, 1997.

[6] D. Plant, B. R. Robertson, H. S. Hinton, G. C. Boisset, N. H. Kim, Y. S. Liu, M. R. Otazo, D. R. Rolston, A. Z. Shang, and W. M. Robertson, "Micro-channel based optical backplane demonstrators using FET-SEED smart pixel array," in *Proc. SPIE*, vol. 2400, 1995, pp. 170–174.

[7] R. T. Chen, L. Wu, F. Li, S. Tang, M. Dubinovsky, J. Qi, C. L. Schow, J. C. Campbell, R. Wickman, B. Picor, M. Hibbs-Brenner, J. Bristow, Y. S. Liu, S. Rattan, and C. Noddings, "Si CMOS process compatible guided-wave multi-Gbit/sec optical clock signal distribution system for Cray T-90 supercomputer," in *Proc. 4th Int. Conf. Massively Parallel Processing Using Optical Interconnects*, Montreal, P.Q., Canada, June 22–24, 1997, pp. 10–24.

[8] T. Suhara and H. Nishihara, "Integrated optics components and devices using periodic structures," *IEEE J. Quantum Electron.*, vol. 22, no. 6, pp. 845–867, 1996.

[9] D. Brundrett, E. Glystis, and T. Gaylord, "Homogeneous layer models for high-spatial-frequency dielectric surface-relief gratings," *Appl. Opt.*, vol. 33, no. 13, pp. 2695–2760, 1994.

[10] D. Y. Kim, S. K. Tripathy, L. Li, and J. Kumar, "Laser-induced holographic surface relief gratings on nonlinear optical polymer films," *Appl. Phys. Lett.*, vol. 66, no. 10, pp. 1166–1168, 1995.

[11] R. T. Chen, F. Li, M. Dubinovsky, and O. Ershov, "Si-based surface-relief polygonal gratings for 1-to-many wafer-scale optical clock signal distribution," *IEEE Photon. Technol. Lett.*, vol. 8, no. 8, 1996.

[12] R. K. Kostuk, J. W. Goodman, and L. Hesselink, "Design considerations for holographic optical interconnects," *Appl. Opt.*, vol. 26, pp. 3947–3953, 1987.

[13] G. D. Boyd, L. A. Coldren, and F. G. Storz, "Directional reactive ion etching at oblique angles," *Appl. Phys. Lett.*, vol. 36, no. 7, pp. 583–585, 1980.

[14] Y. S. Liu, H. S. Cole, J. Bristow, and Y. Liu, "Hybrid integration of electrical and optical interconnects," in *Proc. SPIE*, vol. 2153, 1994, pp. 337–343.

[15] J. Gan, L. Wu, H. Luan, B. Bihari, and R. T. Chen, "Two-dimensional 45-degree surface-normal micro-coupler array for guided-wave optical clock distribution," *IEEE Photon. Technol. Lett.*, vol. 11, pp. 1452–1454, Nov. 1999.

[16] M. Sypek, "Light propagation in the Fresnel region: New numerical approach," *Opt. Commun.*, vol. 116, pp. 43–48, 1995.

[17] J. W. Goodman, *Introduction to Fourier Optics*, 2nd ed. New York: McGraw-Hill, 1996, ch. 4, pp. 63–89.

[18] O. Wada, *Optoelectronic Integration: Physics, Technology, and Applications*. Norwell, MA: Kluwer Academic, 1994.

[19] Y. Sasaki, T. Katayama, T. Koishi, K. Shibahara, S. Yokoyama, S. Miyazaki, and M. Hirose, "High speed GaAs epitaxial lift-off and bonding with high alignment accuracy using a sapphire plate," *J. Electrochem. Soc.*, vol. 146, no. 2, pp. 710–712, 1999.

[20] B. D. Dingle, M. B. Spitzer, R. W. McClelland, J. C. C. Fan, and P. M. Zavracky, "Monolithic integration of a light emitting diode array and a silicon circuit using transfer process," *Appl. Phys. Lett.*, vol. 62, no. 22, pp. 2760–2762, 1993.

[21] E. Yablonovitch, T. Sands, D. M. Hwang, I. Schnitzer, T. J. Bmitter, S. K. Shastry, D. S. Hill, and J. C. C. Fan, "Van der walls bonding of GaAs on Pd leads to a permanent, solid-phase-topotaxial metallurgical bond," *Appl. Phys. Lett.*, vol. 59, no. 24, pp. 3159–3161, 1991.

[22] H. Rosenzweig, M. Ludwig, W. Benz, M Berroth, A. Hulsmann, G. Kaufel, B. Raynor, and J. Schneider, "8.2 GHz monolithic integrated optoelectronic receiver using MSM photodiode and 0.5 μm recessed-gate AlGaAs/GaAs-HEMTs," *Electron. Lett.*, vol. 27, pp. 734–735, 1991.

[23] A. Ketterson, J. W. Seo, M. Tong, K. Nummila, D. Ballegeer, S. M. Kang, K. Y. Cheng, and I. Adesia, "A 10 GHz bandwidth pseudomorphic GaAs/InGaAs/AlGaAs MODFET-based OEIC receiver," presented at the 50th Devices Res. Conf., Cambridge, MA, 1992, VIB-5.

[24] J. S. Wang, C. G. Shih, W. H. Chang, J. R. Middleton, P. J. Apostolakis, and M. Feng, "11 GHz bandwidth optical integrated receivers using GaAs MESFET and MSM technology," *IEEE Photon. Technol. Lett.*, vol. 5, pp. 316–318, 1993.

[25] D. Hartman, M. Grace, and C. Ryan, "A monolithic silicon photo-detector/amplifier IC for fiber and optics application," *IEEE J. Lightwave Technol.*, vol. LT-3, pp. 729–739, 1985.

[26] J. Y. L. Ho and K. S. Wang, "Bandwidth enhancement in silicon metal-semiconductor-metal photodector by trench formation," *IEEE Photon. Technol. Lett.*, vol. 8, pp. 1064–1067, 1996.

[27] J. W. Goodman, F. I. Leonberger, S. Y. Kung, and R. A. Athale, "Optical interconnections for VLSI systems," *Proc. IEEE*, vol. 72, pp. 850–866, 1984.

[28] M. R. Feldman, S. C. Esener, C. C. Guest, and S. H. Lee, "Comparison between optical and electrical interconnects based on power and speed considerations," *Appl. Opt.*, vol. 27, pp. 1742–1751, 1988.

[29] F. E. Kiamilev, P. Marchand, A. V. Krishnamoorthy, S. C. Esener, and S. H. Lee, "Performance comparison between optoelectronic and VLSI multistage interconnects networks," *IEEE J. Lightwave. Technol.*, vol. 9, pp. 1674–1692, 1993.

[30] P. Cinato and K. C. Young, Jr., "Optical interconnections within multichip modules," *Opt. Eng.*, vol. 32, pp. 852–860, 1993.

[31] B. D. Clymer and J. W. Goodman, "Optical clock distribution to silicon chips," *Opt. Eng.*, vol. 25, pp. 1103–1108, 1986.

[32] S. Tang, R. T. Chen, and M. Peskin, "Packing density and interconnection length of a highly parallel optical interconnect using polymer-based single-mode bus arrays," *Opt. Eng.*, vol. 33, pp. 1581–1586, 1994.

[33] R. T. Chen, S. Tang, T. Jannson, and J. Jannson, "A 45 cm long compression molded polymer-based optical bus," *Appl. Phys. Lett.*, vol. 63, pp. 1032–1034, 1993.

[34] R. T. Chen, "Polymer-based photonic integrated circuits," *Opt. Laser Technol.*, vol. 25, pp. 347–365, 1993.

[35] R. T. Chen, H. Lu, D. Robinson, M. Wang, G. Savant, and T. Jannson, "Guided-wave planar optical interconnects using highly multiplexed polymer waveguide holograms," *IEEE J. Lightwave. Technol.*, vol. 10, pp. 888–897, 1992.

[36] R. W. Wickman, "Implementation of optical interconnects in GigaRing supercomputer channel," in *Proc. SPIE*, vol. CR62, 1996, pp. 343–356.
[37] S. Tang and R. T. Chen, "1-to-42 optoelectronic interconnection for intra-multichip-module clock signal distribution," *Appl. Phys. Lett.*, vol. 64, pp. 2931–2933, 1994.
[38] L. Wu, F. Li, S. Tang, B. Bihari, and R. T. Chen, "Compression-molded three dimensional tapered polymeric waveguides for low-loss optoelectronic packaging," *IEEE Photon. Technol. Lett.*, vol. 9, no. 12, pp. 1601–1603, 1997.
[39] Y. Li, J. Popelek, L. J. Wang, Y. Takiguchi, T. Wang, and K. Shum, "Clock delivery using laminated polymer fiber circuits," *J. Opt. A* , vol. 1, pp. 239–243, 1999.
[40] Y. Li, T. Wang, J.-K. Rhee, and L. J. Wang, "Multi-gigabits per second board-level clock distribution schemes using laminated end-tapered fiber bundles," *IEEE Photon. Technol. Lett.*, vol. 10, pp. 884–886, 1998.
[41] Y. Li and T. Wang, "Distribution of light power and optical signals using embedded mirrors inside polymer optical fibers," *IEEE Photon. Technol. Lett.*, vol. 8, pp. 1352–1354, 1996.
[42] P. Sweazey, "Limits of performance of backplane buses," in *Digital Bus Handbook*, J. De Giacomo, Ed. New York: McGraw-Hill, 1990.
[43] R. T. Chen, "VME optical backplane bus for high performance computer," *Jpn. J. Optoelectron.*, vol. 9, pp. 81–94, 1994. Special Issue on Optoelectronic Integrated Circuits.

Ray T. Chen (Senior Member, IEEE) is the Temple Foundation Endowed Professor in the Department of Electrical and Computer Engineering at the University of Texas, Austin. His research group has been awarded more than 60 research grants and contracts from such sponsors as DOD, NSF, DOE, NASA, the State of Texas, and private industry. The research topics include guided-wave and freespace optical interconnects, polymer-based integrated optics, a polymer waveguide amplifier, graded index polymer waveguide lenses, active optical backplanes, traveling-wave electrooptic polymer waveguide modulators, optical control of phased-array antenna, GaAs all-optical crossbar switch, holographic lithography, and holographic optical elements. The optical interconnects research group at UT Austin has reported its research in more than 250 published papers. He has chaired or been a program-committee member for more than 40 domestic and international conferences organized by SPIE (The International Society of Optical Engineering), OSA, IEEE, and PSC. He has served as a Consultant for various federal agencies and private companies and delivered numerous invited talks to professional societies.

Dr. Chen is a Fellow of the SPIE and of the Optical Society of America. He is a Senior Member of IEEE/LEOS and a member of PSC. Currently, there are 20 Ph.D. degree students and seven post-doctors working in Chen's group.

Lei Lin received the B.S. degree from the Department of Material Science, Lanzhou University, China. He received the master's degree in material engineering from the Material Research Center at Norfolk State University, where he investigated laser crystal growth. He also received the master's degree from the University of North Carolina, where he pursued VLSI design in the Electrical and Computer Engineering Department. He is currently a graduate student in electrical and computer engineering at the University of Texas at Austin.

His research topic is integration of thin-film MSM photodetectors in guided wave optoelectronic interconnects.

Chulchae Choi received the B.S. and M.S. degrees in physics from Inha University, Korea, in 1989 and 1991, respectively.

From 1991 to 1998, he performed research in organic photoconductor, ladar, optical pickup, and solid-state lasers. He is now a Graduate Researcher in electrical and computer engineering at the University of Texas at Austin. His interests are in the area of optical interconnects. His current research projects deal with fully embedded board-level optical interconnects.

Yujie J. Liu received the B.S. and M.S. degrees in electronic science from Nankai University, Tianjin, China, in 1995 and 1998, respectively. She is currently pursuing the Ph.D. degree in electrical engineering at the University of Texas at Austin.

Her area of research is guided-wave optical interconnects.

Bipin Bihari received the Ph.D. degree in physics (laser spectroscopy) from the Indian Institute of Technology, Kanpur, India.

Presently, he is working as a Research Scientist jointly at Radiant Research, Inc., and at the Microelectronics Research Center of the University of Texas at Austin. He is the author or coauthor of more than 45 articles in refereed journals and conference proceedings. His areas of interest include optoelectronic interconnects, WDM for data-com applications, optical memories, polymeric waveguides and devices, molded waveguides, nanophase materials, and nonlinear optical properties of organic and inorganic materials. Dr. Bihari is a member of several professional societies, including ACS, MRS, SPIE, and IMAPS. He has served as the session chair at several conferences organized by SPIE.

L. Wu, photograph and biography not available at time of publication.

Suning Tang, (Member, IEEE) received the B.S. degree in electrical engineering (laser devices) in China, the master's degree in fiber optics from the Weizmann Institute of Science in Israel, and the Ph.D. degree in electrical engineering (optoelectronic interconnects) from the University of Texas at Austin, in 1994. He is Chief Scientist at Radiant Research, Inc., Austin, TX. He worked for Cirrus Logic (Crystal Semiconductors) and Advanced Photonics Technologies for four years before he joined Radiant Research, Inc. His work in the past 15 years includes optical interconnects, WDM devices, fiber-optic devices, optical waveguide modulators/switches, optical control of microwave signals, and semiconductor photonic devices. He has been the Co-principal Investigator for more than 25 SBIR research programs awarded by the Department of Defense and private industry. He has served as Conference Chairman for several SPIE international conferences. He has published more than 80 papers in IEEE, OSA, AIP, and SPIE journals, and has several Patents pending.

Dr. Tang is a Member of SPIE and OSA.

R. Wickman, photograph and biography not available at time of publication.

B. Picor, photograph and biography not available at time of publication.

M. K. Hibbs-Brenner received the B.A. degree in physics from Carleton College, Northfield, MN, and the M.S. and Ph.D. degrees in material science from Stanford University, Stanford, CA.

She is currently the Manager of the Photonics group at the Honeywell Technology Center, Minneapolis, MN, The Photonics group develops optoelectronic component integration and packaging technology for data communication and optical sensing applications. She has been involved in the development of vertical-cavity surface-emitting lasers and smart pixel technology for the past ten years. She is the author or co-author of more than 30 journal publications, and numerous invited and contributed conference presentations.

Dr. Hibbs-Brenner is a member of the IEEE Lasers and Electro-Optics Society.

J. Bristrow, photograph and biography not available at time of publication.

Y. S. Liu, photograph and biography not available at time of publication.